

Tremor mapping at the Groningen field



Universiteit Utrecht

Elmer Ruigrok, Hanneke Paulssen and Jeannot Trampert

Department of Earth Sciences, Utrecht University, Utrecht, The Netherlands, (contact address: e.n.ruigrok@uu.nl)

1. Regional setting

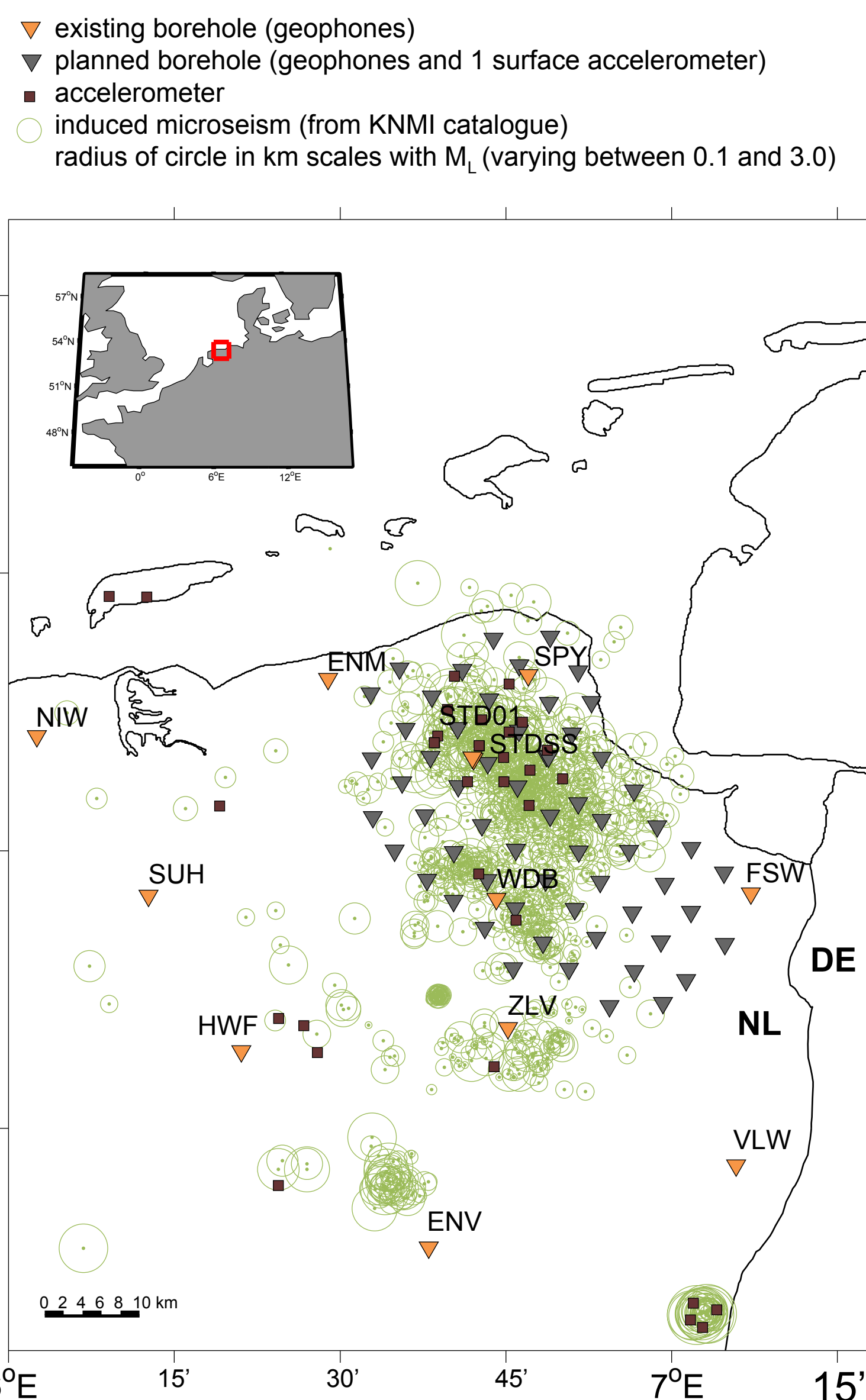


Fig. 1: An overview of induced seismicity (green circles) in the NE part of the Netherlands. Most seismicity is confined to the Groningen gas field. Event locations were obtained by the Royal Netherlands Meteorological Institute (KNMI), with a borehole geophone network (orange triangles) and accelerometer network (purple squares). A new recording network (grey triangles) has been planned and partly constructed.

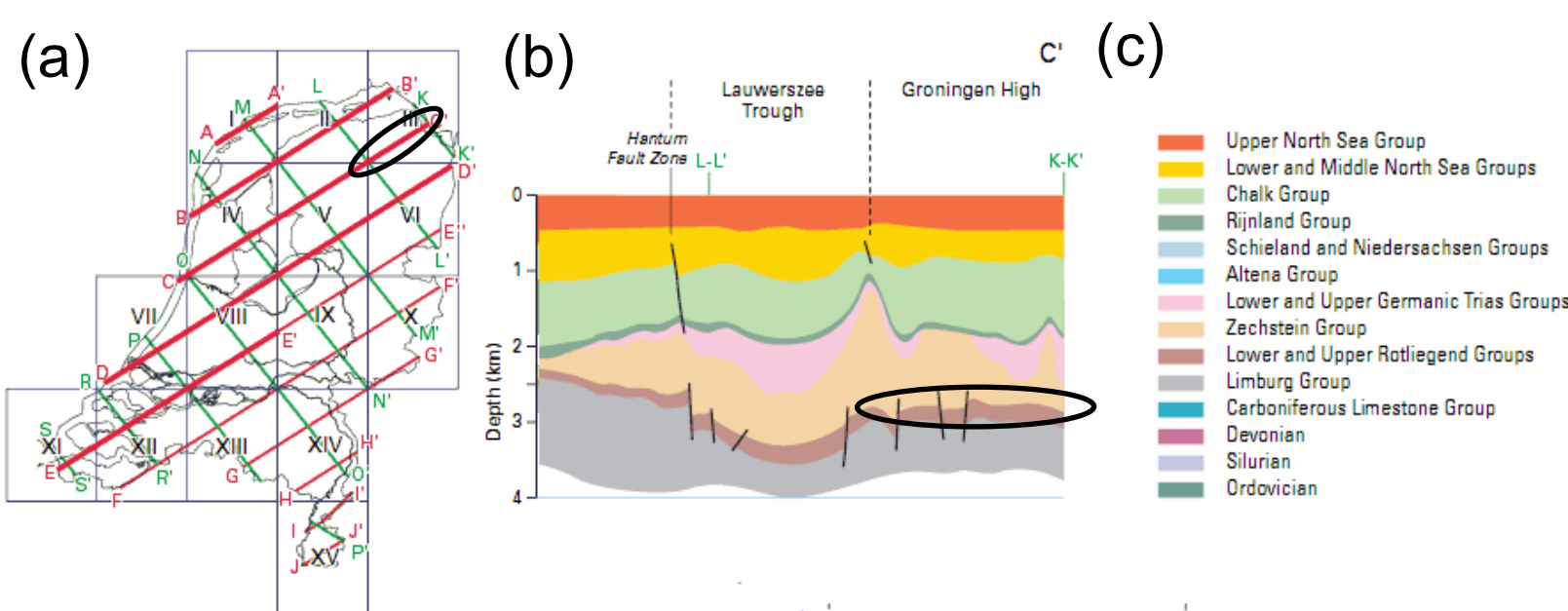


Fig. 2: (a) a map of the Netherlands with available sections (red and green lines) of ~ the upper 4 km of the subsurface. Highlighted with a black oval is a section that covers the Groningen gas field. (b) shows this section and (c) is a legend for the different geological strata on (b). The gas reservoir is a sandstone from the Rotliegendes Group, as highlighted by a black oval. The caprock is salt from the Zechstein Group. The reservoir is compartmented by numerous faults. The area shows significant 3D structure, mainly due to salt doming. The subsurface below the reservoir is not well known.

Source: TNO

Abstract

The Groningen gas field is a giant natural gas accumulation in the northeastern part of the Netherlands. The gas is present in a reservoir at a depth of about 3 km. The gas-filled sandstone extends about 45 by 25 km laterally and 140 m vertically. Decades of production have led to significant compaction of the sandstone. The (differential) compaction is thought to re-activate existing faults and therewith to be the main driver of induced seismicity (NAM, 2013).

The current seismic network (Fig. 1) has been designed to detect and locate all (impulsive) events with $M_L > 1.5$ (van Eck et al., 2006). Precise location is difficult due to a complicated subsurface. Amongst others, the induced wavefield is perturbed by a heterogeneous salt layer on top of the reservoir. Likely due to unprecise location, the current hypocentre estimates do not clearly correlate with a well-known fracture network (Kraaijpoel and Dost, 2013). Our current research focuses on detecting also the non-impulsive seismicity and finding preferential locations of these tremors. This could lead to identification of the reactivated faults.

On this poster, we show a strategy for automatic location and detection of small-magnitude seismicity, for which no template is present. From past seismicity, we assimilate one average shotgather and determine from it the average horizontal velocity of the first arriving P-wave refraction. Next, we use the recordings over borehole arrays to accentuate packages of up-going P-waves. From these packages we stress the onsets using kurtosis. The kurtosis traces are then crosscorrelated and time-difference migrated to yield maps of potential seismic activity. Due to borehole stacking, kurtosis computation and array stacking (migration), these maps are expected to contain events that are hidden below the noise level on individual seismograms. However, we did not yet fully implement the above strategy to confirm this with field data.

2. Velocity estimation

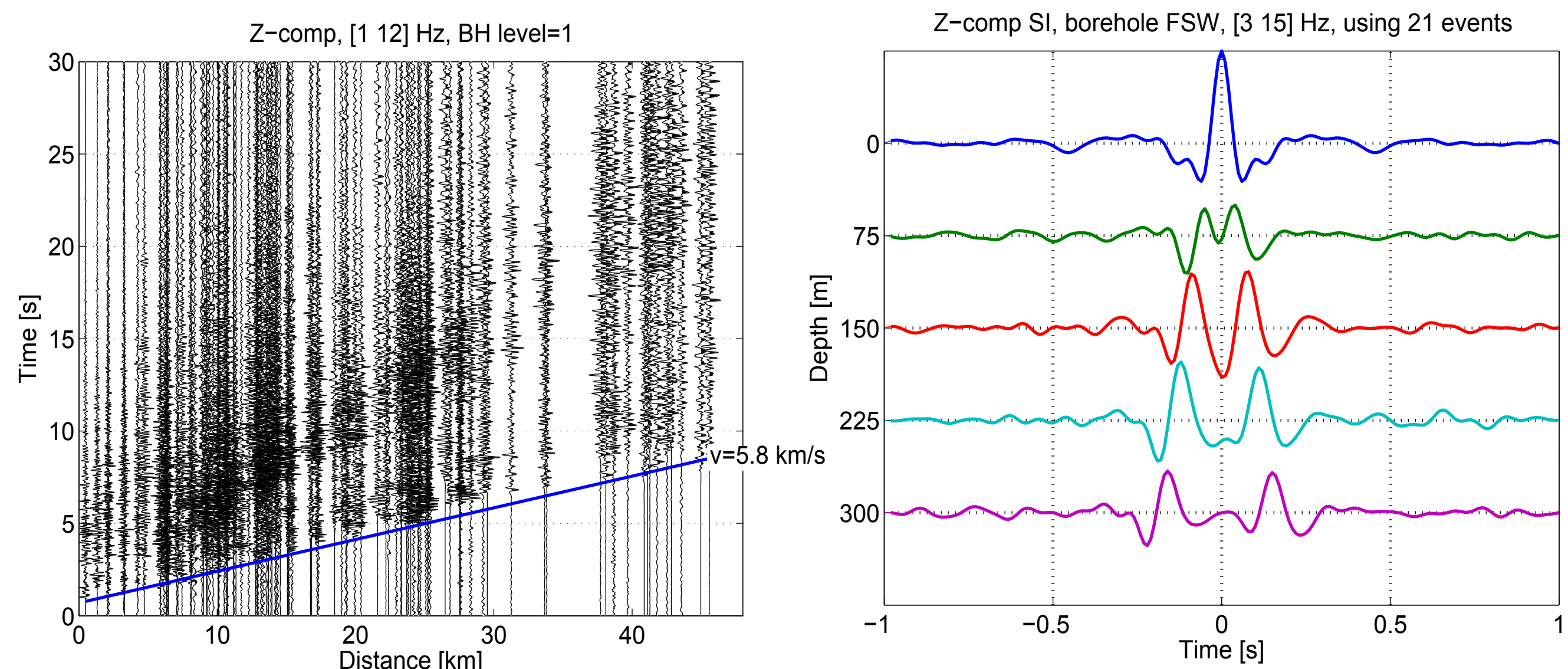


Fig. 3: Seismograms plotted as function of distance from sources. From multiple events and borehole stations in the Groningen area (Fig. 1) vertical-component seismograms were selected with high signal-to-noise ratio. The picked average horizontal velocity (blue line, 5.8 km/s) primarily corresponds to a refraction over a layer below the reservoir. Likely, the main refraction is over the Carboniferous Limestone Group (Fig. 2).

Fig. 4: To determine seismic velocities over the boreholes, we use seismic interferometry (Wapenaar et al., 2010). Above we show an example for the vertical components of borehole FSW (Fig. 1). We apply seismic interferometry to 21 events recorded over the borehole array. By doing so, we retrieve the response as if there were a (P-wave) source at the Earth's surface (at the upper borehole station), which response were measured by the other stations in the borehole. The retrieved responses are shown on the above figure. They contain contributions at negative and positive times, which result from upgoing and downgoing waves, respectively. Picking the direct waves yields average velocities between the sensor positions. For the 4 intervals, from top to bottom, this gives 1.5, 2.1, 2.1 and 2.0 km/s, respectively.

3. Processing flow

Time window of vertical-component seismic recordings over the array

Emphasize P-wave onsets

1. For each borehole station, add time shifts to data corresponding to delay times of upgoing P-wave (Fig. 4)
2. Sum time-shifted data over borehole array elements (Fig. 6c)
3. Compute the derivative of the kurtosis of the shifted and summed borehole data (Fig. 7c)

Data reduction

1. Crosscorrelation of resulting kurtosis traces over the different borehole arrays.
2. Remove delay times larger than the maximum time difference over the array for an earthquake at the Groningen field.

Location and detection

1. Traveltime-difference migration of the data-reduced traces (Fig. 8)
2. Application of imaging condition

Map with likely source locations

5. Location

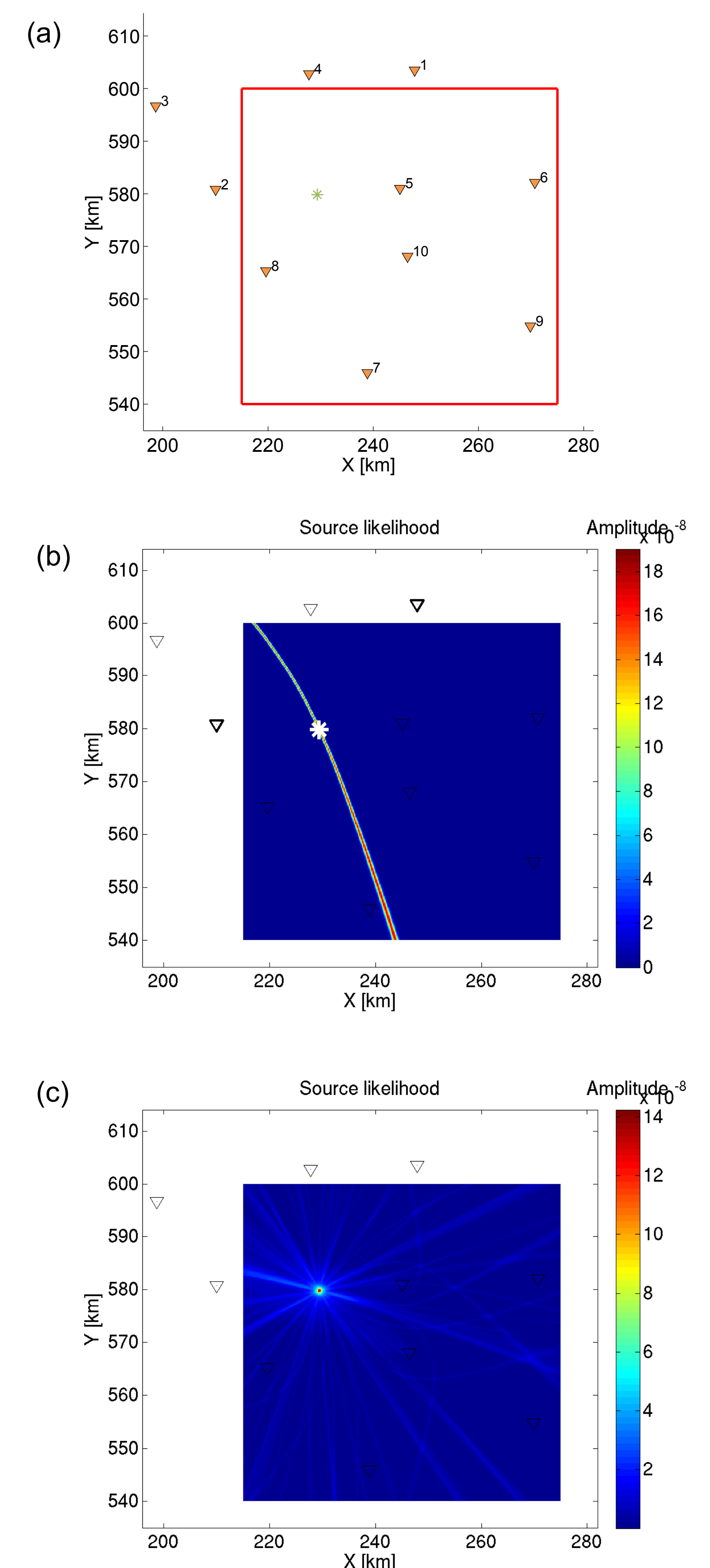


Fig. 8: (a) shows the Groningen borehole array network (Fig. 1) in a local coordinate system (Rijksdriehoekstelsel). Triangles denote receiver locations, and the star denotes a source. The red square borders the search grid for which the presence of sources will be evaluated. For a source at the star, the waveforms are forward modelled. Subsequently, the kurtosis is taken and the kurtosis traces are cross-correlated over the array. (b) Shows the result of time-difference migrating the crosscorrelation result for a single station pair (as highlighted by bold triangles). (c) Shows the migration result for all station combinations.

4. Emphasis of P-wave onsets

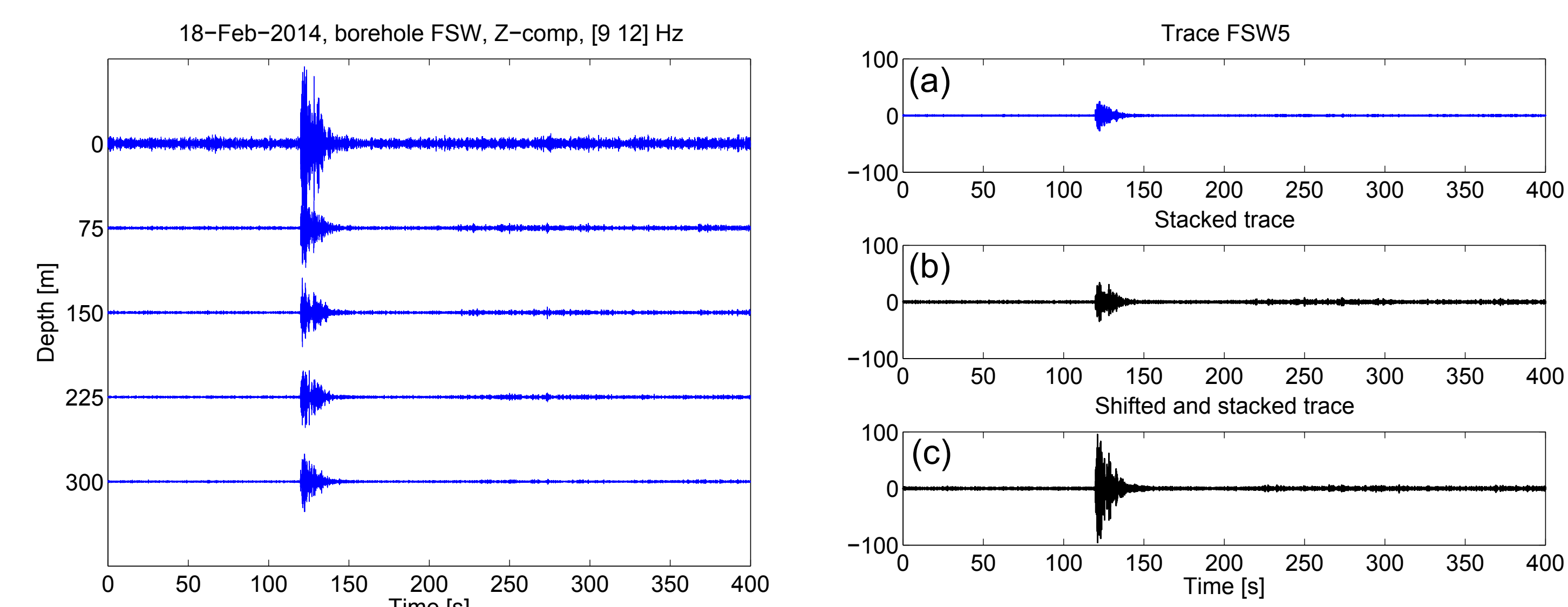


Fig. 5: (a) a 400 s vertical-component recording over the FSW borehole array (Fig. 1). The time window includes a clear earthquake response (Westerwijterd event, with a local magnitude of 1.7, measured at a distance of 33.4 km. The signal-to-noise ratio increases with depth.

Fig. 6: (a) repeats the measurement from Fig. 5 at 300 m depth. To this seismogram we compare (b) a simple stack over all seismograms in Fig. 5, but for the one at the free surface and (c) a stack of the same seismograms after shifting the traces using the P-wave velocity as found in Fig. 4. Trace (c) emphasizes up-going P-waves. Because of low velocities in the (unconsolidated) near surface, P-waves due to source at depth will propagate nearly vertically along the borehole array and are thus stacked in constructively after the shifting operation.

Fig. 7: To stress only the onset of the event, we compute the positive derivative of the kurtosis of the traces in Fig. 6. The kurtosis can be seen as an alternative to short-time average over long-time average, which alternative works well in high-scattering environments, like volcanoes (Langet et al., 2014). Note that (c), the kurtosis measure of the shifted and stacked trace, is the highest.

Acknowledgements

We kindly acknowledge the Royal Netherlands Meteorological Institute (KNMI) for providing us with field data and for good discussions. The research is supported by the Sustainability / Geo-Resources Programme of Utrecht University.

References

- Kraaijpoel, D., & Dost, B. (2013). Implications of salt-related propagation and mode conversion effects on the analysis of induced seismicity. *Journal of seismology*, 17(1), 95-107.
- Langet, N., Maggi, A., Michelini, A. & Breneguier, F. (2014). Continuous kurtosis-based migration for seismic event detection and location, with application to Piton de la Fournaise Volcano, La Reunion. *Bulletin of the Seismological Society of America*, 104(1), 229-246.
- Van Eck, T., Goutbeek, F., Haak, H., & Dost, B. (2006). Seismic hazard due to small-magnitude, shallow-source, induced earthquakes in The Netherlands. *Engineering Geology*, 87(1), 105-121.
- Wapenaar, K., Draganov, D., Snieder, R., Campman, X. & Verdel, A. (2010). Tutorial on seismic interferometry: Part 1 — Basic principles and applications. *Geophysics*, 75(5), 75A195-75A209.